EDGE ARTICLE

Check for updates

Far-red/near-infrared emitting, two-photon absorbing, and bio-stable amino-Si-pyronin dyes†

Kyeong Hwan Kim,[a] Subhankar Singha, [ID] *[a] Yong Woong Jun, [ID] [a] Ye Jin Reo, [ID] [a] Hye Rim Kim,[a] Hye Gun Ryu,[a] Snehasis Bhunia[b] and Kyo Han Ahn [ID] *[a]

Organic fluorophores emitting in the far-red/near-infrared (NIR) wavelength region are in great demand for minimal autofluorescence and reduced light scattering in deep tissue or whole body imaging. Currently, only a few classes of far-red/NIR fluorophores are available including widely used cyanine dyes, which are susceptible to photobleaching and form nonfluorescent aggregates. Even rare are those far-red/NIR emitting dyes that have two-photon imaging capability. Here we report a new class of far-red/NIR-emitting dyes that are photo-stable, very bright, biocompatible, and also two-photon absorbing. The introduction of an electron-withdrawing group such as *N*-acyl or *N*-alkoxycarbonyl groups on the C-10-amino substituent of the new julolidine-derived amino-Si-pyronin dyes (ASiP^j), which emit in the far-red region, causes large bathochromic shifts, leading to NIR-emitting amino-Si-pyronin dyes (NIR-ASiP^j) having high cellular stability. Furthermore, the ASiP^j–NIR-ASiP^j couple offers a novel ratiometric bioimaging platform with a large spectral gap, as demonstrated here with a boronate-containing NIR-ASiP^j derivative that is converted to the corresponding ASiP^j dye upon reaction with hydrogen peroxide.

Introduction

Fluorescence imaging offers a powerful means in modern science for studying and visualizing complex biological systems.[1,2] The promising features of fluorescence imaging in turn have inspired a quest for novel fluorophores and molecular probes with desirable photophysical properties. A fluorescent molecule desirable for bioimaging application should be excitable and also emissive in the longer wavelength region, preferably from the far-red to near-infrared (NIR) region (650–950 nm), in order to minimize phototoxicity and background fluorescence from biomolecules (autofluorescence).[3–5] NIR emitting cyanine dyes are widely used for bioimaging; however, they suffer from drawbacks such as photobleaching[6] and also from susceptibility to form nonfluorescent aggregates.[7] Therefore, the development of a new class of dyes with desirable photophysical properties is in great demand but remains a challenge. Furthermore, even rare are the far-red/NIR emitting

dyes with two-photon imaging capability, which are in great demand for long-term monitoring of biological analytes with minimal autofluorescence.[8,9]

Recently, Nagano and co-workers developed a family of far-red/NIR fluorescent rhodamine analogues including Si-rhodamine dyes (SiR),[10] since the first report on the Si-pyronin (SiP) core by Xiao, Qian and co-workers.[11] Silicon analogues still possess the optical properties of the original rhodamine dyes, such as high fluorescence quantum yields, photostability and cell permeability. Accordingly, SiR dyes have recently received significant attention for the development of fluorescent probes[12] and fluorescence imaging techniques including super-resolution imaging and multicolor imaging.[13–16] These conventional SiR dyes, which mostly emit in the far-red region, however, show very small Stokes shifts ($\Delta\lambda = \sim$18 nm),[14] similar to BODIPY ($\Delta\lambda = \sim$10 nm)[17] and rhodamine dyes ($\Delta\lambda = \sim$20 nm),[18] which raises the light reabsorption issue in bioimaging. Also, they have been rarely used for two-photon microscopy imaging,[19] a powerful means for obtaining high-resolution 3D images of living specimens (including animal tissues) down to the depth of a millimeter along with reduced photo-damage and photo-bleaching.[20,21]

The fact that the conversion of BODIPY and rhodamine to the corresponding amino-BODIPY[22] and amino-pyronin[23,24] dyes shows large Stokes shifts ($\sim$60 and $\sim$105 nm, respectively) and good two-photon absorbing properties[25,26] prompted us to investigate the corresponding amino-Si-pyronin (ASiP) dyes and their derivatives. Earlier, a structurally simple 10-amino-Si-xanthene precursor was used to synthesize *N*-acylated-

[a]*Department of Chemistry, Pohang University of Science and Technology (POSTECH), 77 Cheongam-Ro, Nam-Gu, Pohang, Gyeongbuk 37673, Republic of Korea. E-mail: subhankar@postech.ac.kr; ahn@postech.ac.kr*

[b]*National Institute for Nanomaterials Technology (NINT), Pohang University of Science and Technology, 77 Cheongam-Ro, Nam-Gu, Pohang, Gyeongbuk 37673, Republic of Korea*

† Electronic supplementary information (ESI) available: Supporting figures and schemes, experimental procedures for the measurement of one-photon and two-photon photophysical properties, cell viability assay, and detailed synthesis and characterization data of the new dyes and probe. See DOI: 10.1039/c9sc02287b

iminoanthrone derivatives by Klán and co-workers.[27] In the course of our study,[28] Butkevich *et al.* reported alkylamino-Si-pyronin dyes and their application to super-resolution fluorescence microscopy.[29] Also, Guo and co-workers subsequently reported ASiP dyes with two-photon imaging application.[30] We noticed that even though it was possible to induce large Stokes shifts and two-photon imaging capability by converting the "conventional" SiR dye system into the corresponding ASiP system, unfortunately, the reported ASiP analogues showed hypsochromic shifts in their emission and absorption spectra ($\Delta\lambda = \sim$50 nm in a buffer solution) from the corresponding SiR dyes. Accordingly, the ASiP dyes known so far showed the maximum emission wavelength (λ_{em}) of around $\sim$610 nm, which belongs to the orange emission region, which would cause significant autofluorescence.[8,9] To address this critical issue, it is necessary to develop fluorophores that emit in the far-red/NIR region. Currently, only a few classes of such dyes are available, which are mostly based on cyanines,[31] BODIPYs,[32] hemicyanine hybrids of rhodamines, fluoresceins and coumarins,[33] silicon-based rhodamines,[34] and benzocoumarins.[8] To this end, we undertook a rational approach to develop a novel class of two-photon active, NIR-emitting ASiP derivatives (NIR-ASiP). At the same time, we also intended to modulate the photophysical properties of new ASiP dyes by implementing an "activable" functional group by an analyte or a stimulus, which would ultimately provide a ratiometric bioimaging platform (Fig. 1a). Although rhodamine and Si-rhodamine dyes have been widely used for the development of fluorescent probes,

they mostly operate in the turn-on sensing mode through the lactam ring-opening process. For reliable and quantitative analysis, a ratiometric probe that shows signals at two different wavelengths with a large spectral separation is highly promising, as it avoids environmental and instrumental effects on fluorescence change.[35] Herein, we disclose NIR-emitting ASiP dyes and their parent ASiP dyes, the couple of which also constitutes a promising ratiometric bioimaging platform with large spectral shifts.

Results and discussion

Design and development of amino-Si-pyronin based two-photon absorbing NIR emitting dyes

We reasoned that introducing an amine donor at C-10 of SiP dyes may impart electronic perturbation and intramolecular charge transfer (ICT) characteristics to the resulting dyes, which may endow them with two-photon absorbing properties as in the case of the amino-BODIPY system.[25,26] In a further approach, modulating the electron-donating ability of the 10-amino group may induce bathochromic spectral shifts. Both approaches indeed ultimately have led to two-photon active, NIR-emitting Si-pyronin analogues.

Thus, starting from a bis(dimethylamino)-Si-xanthone intermediate (for its synthesis, see the ESI†), we synthesized various amino-Si-pyronin compounds (ASiP[a] **1–10**; Tables 1 and S1, ESI†) by introducing different types of alkylamines at C-10 of the Si-pyronin core. Then, the electron-donating ability of the
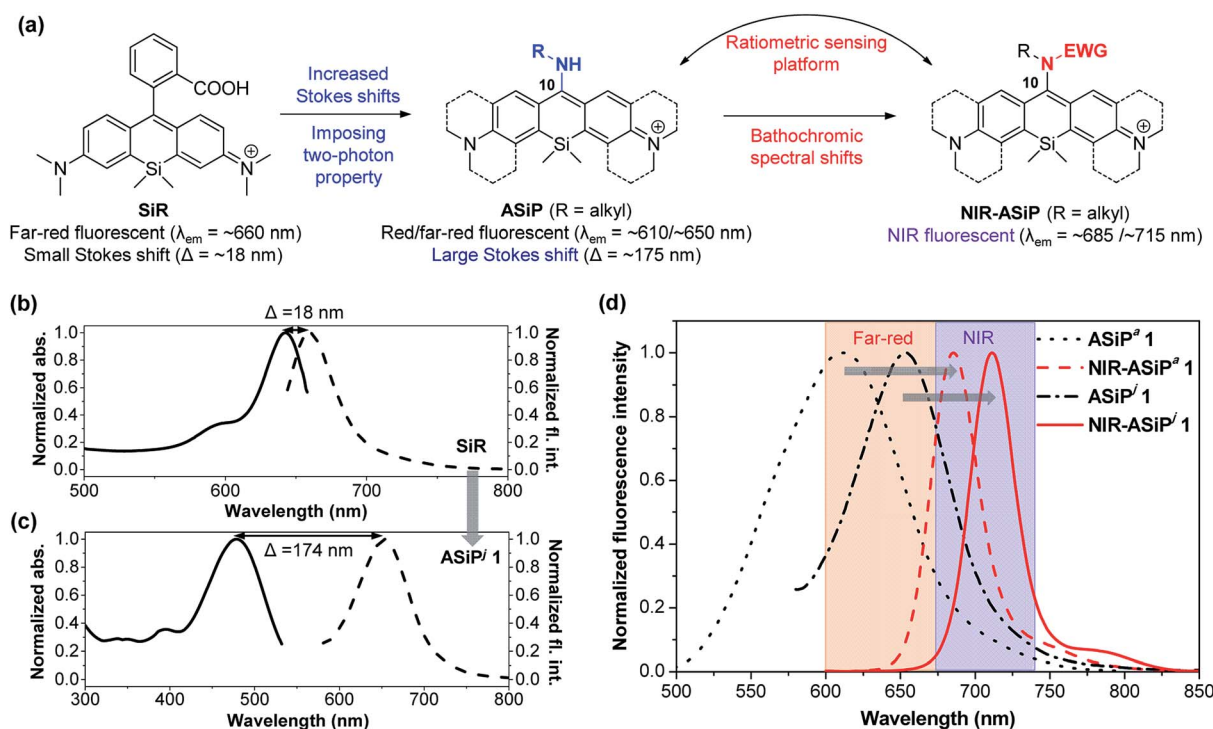

Fig. 1 (a) The design strategy used for NIR-emitting amino-Si-pyronin (NIR-ASiP) dyes as well as a ratiometric sensing platform. EWG = electron-withdrawing group. (b and c) Normalized absorption (solid line) and emission (dash line) spectra of SiR (b) and ASiP[j] **1** (c) in PBS (pH 7.4) containing 1% DMSO. (d) Emission spectral shift of ASiP dyes to NIR-ASiP dyes in PBS (pH 7.4) containing 1% DMSO. The emission spectra were obtained by excitation at the maximum absorbance wavelength of each dye.

Table 1 Photophysical properties of ASiP[a] and NIR-ASiP[a] analogues

(Alkyl) $R_1 \backslash N / R_2$ (EWG)

ASiP[a] / NIR-ASiP[a]

R_1-N-R_2: Cyclic urea =

	R_1 (alkyl)	R_2 (EWG)	$\lambda_{abs}{}^a$/nm	$\lambda_{em}{}^b$/nm	$\Phi_F{}^c$
ASiP[a] 1	Me	H	452	612	0.33[d]
ASiP[a] 2	Bn	H	469	623	0.34[e]
ASiP[a] 3	Propargyl	H	473	628	0.25[e]
NIR-ASiP[a] 1	Me	CO_2Bn	669	685	0.42[f]
NIR-ASiP[a] 2	Propargyl	$COCH_3$	676	694	0.31[e]
NIR-ASiP[a] 3	Propargyl	$COCF_3$	684	707	0.27[e]
NIR-ASiP[a] 4	Propargyl	SO_2CF_3	694	713	0.25[e]
NIR-ASiP[a] 5	Bn	$COCF_3$	684	704	0.29[e]
NIR-ASiP[a] 6	Cyclic urea		674	690	0.22[e]

[a] Maximum absorption wavelength. [b] Maximum emission wavelength in PBS (pH 7.4). [c] Fluorescence quantum yield. [d] Determined in methanol using fluorescein as the reference (Φ_F = 0.95 in 0.1 M NaOH).[18] [e] Determined in ethanol using rhodamine 101 (Φ_F = 0.915 in EtOH) as the reference dye. [f] Determined in CH_3CN using Nile blue (Φ_F = 0.27 in ethanol) as the reference dye.

10-amino group was further modulated by attaching an electron-withdrawing group (EWG) to it, which provided the NIR-emitting ASiP[a] analogues.

The photophysical properties of ASiP[a] 1–10 measured in PBS (containing 1% DMSO) show the one-photon absorption maxima at around 450–475 nm while the corresponding emission maxima at around 600–625 nm (Tables 1 and S1, ESI†). We found that the propargylamine derivative ASiP[a] 3 showed a little red-shift in the absorption and emission bands compared to those of the methylamine and benzylamine analogues, ASiP[a] 1 and 2, which suggested that a further bathochromic shift would be induced by introducing a more electron-withdrawing substituent at C-10. Accordingly, we synthesized a carbamate derivative (NIR-ASiP[a] 1) and measured its photophysical properties. Indeed, NIR-ASiP[a] 1, which is the benzyl carbamate derivative of ASiP[a] 1, exhibited large bathochromic shifts in the absorption and emission bands ($\Delta\lambda$ = 218 nm and 75 nm, respectively) with the maximum intensity peaks at 669 nm and 685 nm, respectively (Table 1 and Fig. S1, ESI†).

Computational calculations (using Gaussian '09) performed for ASiP[a] 1 and a simplified carbamate form NIR-ASiP[a] 1 gave a HOMO–LUMO energy gap of 2.97 eV and 2.41 eV, respectively (Fig. S2, ESI†), supporting the bathochromic spectral shifts upon attaching an electron-withdrawing group to the C-10 amine site. The spectral tuning of such ASiP[a] dyes is thus readily realized by a simple transformation, avoiding laborious and complex synthetic operations.

Bio-stability issues of NIR emitting NIR-ASiP[a] dyes

After characterizing the photophysical properties of the ASiP[a] dyes, we evaluated their cellular imaging capability toward

HeLa cells under one-photon (λ_{ex} = 488 nm) and two-photon excitation (λ_{ex} = 900 nm) conditions. The selected dyes ASiP[a] 2 and ASiP[a] 3 provided very bright images by confocal laser-scanning microscopy (CLSM) (Fig. S3a and b, ESI†) as well as two-photon microscopy (TPM) (Fig. S3c and d, ESI†). The excellent imaging capability of the ASiP[a] dyes under two-photon excitation further confirms their two-photon absorbing properties, as also reported by Guo and co-workers.[30]

Surprisingly, NIR-ASiP[a] 1 showed very dim cellular images when the emission was collected in the far-red/NIR wavelength region of 650–800 nm upon excitation at 633 nm. In contrast, strong emission was observed in the shorter wavelength region of 500–630 nm upon excitation at 488 nm (Fig. 2a, panels A and G). The unexpected cellular imaging results of NIR-ASiP[a] 1 indicated that the NIR-ASiP[a] type dyes are chemically unstable inside cells.

Indeed, NIR-ASiP[a] 5 upon treatment with cysteine (Cys) or glutathione (GSH) in 1 : 1 PBS–dioxane at 37 °C showed little fluorescence in the NIR region, whereas a new emission band at around 600 nm corresponding to ASiP[a] increased as time went (Fig. S4†). The new band was due to the ASiP[a]-type Cys-adduct, as confirmed by HPLC-MS and NMR analyses. The formation of the Cys-adduct also suggests that NIR-ASiP[a] type dyes also react with cellular proteins similarly through thiol addition followed by intramolecular amine substitution (Fig. 2b).[36]

Although the carbamate NIR-ASiP[a] 1 seems to be less reactive that the trifluoroacetyl analogue 5 towards biothiols (Cys and GSH) in the buffer solution (Fig. S5, ESI†), fluorescence from the shorter wavelength window was still observed in the cellular imaging data. This is likely due to the bioconjugation reactions with cellular proteins, as supported by a gel-electrophoresis analysis of A549 cells incubated with NIR-ASiP[a] 1 (10 µM) for
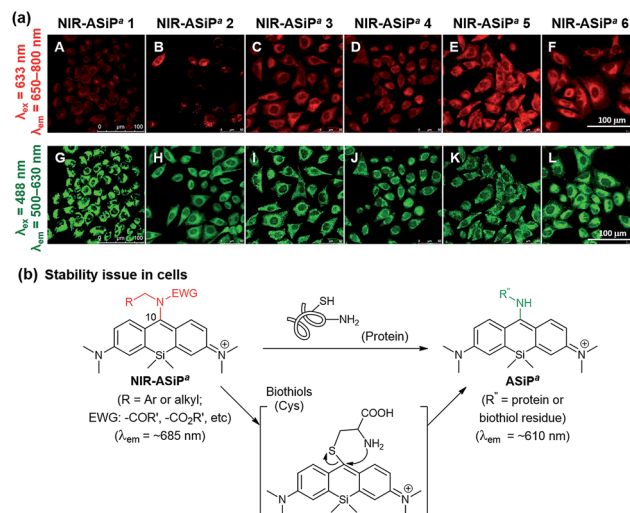

Fig. 2 (a) Images of A549 cells incubated with NIR-ASiP[a] dyes (10 µM) for 30 min. Emission window/excitation wavelength: (A–F) 650–800 nm/633 nm; (G–L) 500–630 nm/488 nm. Scale bar: 100 µm. (b) NIR-ASiP[a] 5 reacts with Cys through thiol substitution followed by amine substitution to form the corresponding ASiP[a]-type product. Similarly, cellular proteins seem to react with NIR-ASiP[a] dyes, plausibly through thiol addition followed by intramolecular amine substitution.
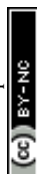
1 h: a strong fluorescence band (broad) appeared, plausibly due to dye-labeled cellular proteins (Fig. S6, ESI†).

To secure the cellular stability of the NIR-ASiP[a] dyes, initially we varied the C-10 amino group. Changing the amino group into the corresponding carboxamide, sulfonamide, cyclic urea, and other functional groups, in all cases, was found to be ineffective in securing the desirable cellular stability (see Table 1 for the dye structures and Fig. 2a for the corresponding cellular images).

Thus, a different approach was necessary to address the cellular instability issue of such NIR-ASiP[a] dyes.

Securing bio-stability through developing julolidine-derived NIR-emitting amino-Si-pyronin dyes

It is known that the C-10 of SiR is more susceptible to nucleophilic attack compared to that of rhodamine dyes. Indeed, the high electrophilicity at the C-10 of SiR was used for the development of a GSH probe[37,38] and for super-resolution imaging.[39–44] Importantly, the electrophilicity at the C-10 of SiR is also dependent on the polarity of the medium: for example, a 2′-carboxy-SiR compound exists mainly in the nonfluorescent spirolactone form in less polar media due to the nucleophilic attack of the nearby carboxylate to the C-10, whereas it exists in the fluorescent zwitterionic form in highly polar media (Fig. 3b).[39–42] Similarly, polarity-dependent electrophilicity at C-10 would be also expected for NIR-ASiP[a] in the cellular matrix, the less polar media compared to the aqueous

buffer solution, plausibly causing the nucleophilic attack by biomolecules (biothiols or amines).

For electronic modulation at C-10, we also compared ASiP[a] derivatives with other amine substituents such as methoxy-amine, phenylhydrazine or benzhydrazide (see Fig. S7 in the ESI† for the dye structures). Unfortunately, all these ASiP[a] analogues showed a tendency to exist in the non-fluorescent form. Introducing a sterically bulky amine such as benzhy-drylamine provided a bright ASiP[a] analogue, but subsequent attempts to attach any electron-withdrawing substituent to the amine site were found to be difficult.

Toward cellular-stable NIR-ASiP dyes, finally we turned our attention to the dye's core structure. Eventually, we were able to overcome the bio-instability of the NIR-ASiP[a] dyes by changing the dye skeleton, from bis(dimethylamino)-SiP (ASiP[a] where a represents the acyclic amine donor) to julolidine-derived SiP (ASiP[j]), as shown in Fig. 3a. In the resultant ASiP[j] dyes, the four alkyl substituents on the Si-xanthene core are expected to increase the electron density at C-10, in addition to increasing the steric hindrance around it. Gratifyingly, these effects together are found to stabilize the corresponding NIR-emitting dyes (NIR-ASiP[j]) from possible nucleophilic attack by biothiols and amines inside cells.

Computational calculations using the Gaussian' 09 program (B3LYP/6-31+G(d)) for ASiP[a] **1** and ASiP[j] **1** showed that the Mulliken charge on the C-10 of ASiP[a] **1** is +0.193 a.u., whereas that of ASiP[j] **1** is −0.143 a.u. Thus, the electrophilicity at C-10 is significantly lowered in ASiP[j] **1** compared to that in ASiP[a] **1**.
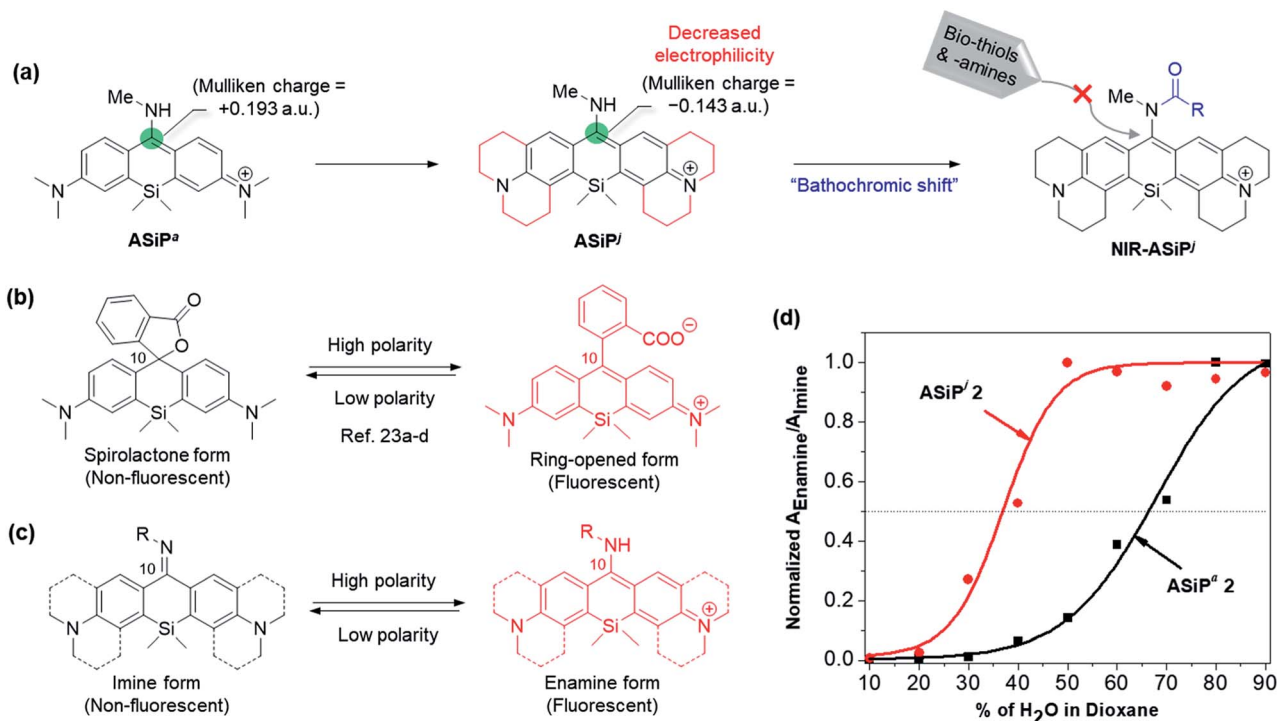

Fig. 3 (a) Far-red emitting julolidine-derived amino-Si-pyronin dyes (ASiP[j]) and their NIR-emitting derivatives (NIR-ASiP[j]) that are stable inside cells. The corresponding Mulliken charges at C-10 of ASiP[a] and ASiP[j] are shown in atomic unit (a.u.). Structural changes of (b) SiR and (c) ASiP dyes depending on the polarity of the medium. (d) Changes of the normalized absorbance ratio of the enamine form (fluorescent) to the imine form (non-fluorescent) depending on the medium polarity (increasing water content in 1,4-dioxane), compared for ASiP[a] **2** and ASiP[j] **2**.

Moreover, the corresponding HOMO–LUMO energy gaps obtained for ASiP[a] **1** and ASiP[j] **1** were −2.97 eV and −2.83 eV, respectively; hence, bathochromic spectral shifts are also expected upon introducing the alkyl substituents.[11]

The ASiP dyes' emission behavior is dependent on the medium polarity.[29] By following the protocol established for carboxyphenyl-substituted Si-rhodamine dyes by Lukinavičius et al.,[39,41] and Butkevich et al.,[40,42] we compared the equilibrium behavior of two selected dyes, ASiP[a] **2** and ASiP[j] **2**, depending on the medium polarity. The ASiP dyes can exist in two forms, the highly conjugated enamine and less conjugated imine forms, of which equilibrium that involves protonation/deprotonation is dependent on the media (Fig. 3c).[29] The enamine form with an extended π-conjugation feature is strongly emissive, whereas the imine form is poorly emissive plausibly due to imine bond isomerization and short π-conjugation. A series of absorption spectra were recorded for the two selected dyes in water–dioxane media by varying the water content and hence the polarity (Fig. S8 and S9, ESI†). The ratio of the enamine to the imine form for each of the ASiP dyes, as represented by the ratio of the corresponding absorbance, is plotted against the medium polarity (Fig. 3d). The data show that half of the ASiP[a] **2**
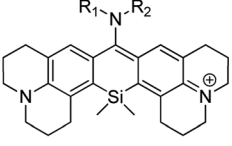
molecules exists in the fluorescent enamine form only in a medium of above 70% water–dioxane, whereas ASiP[j] **2** is expected to remain in the fluorescent form over a wide range of polarity (>37% water–dioxane). Thus, we can conclude that the ASiP[j] skeleton is more electron-rich (that is, the enamine proton is less acidic) than the ASiP[a] skeleton. As a result, the ASiP[j] dyes are expected to show emission behavior even at cytosolic pH values. In contrast, the ASiP[a] dyes fluoresce only in acidic organelles such as lysosomes, but not in the cytosol (at neutral pH).[30]

Photophysical properties of julolidine derived ASiP[j] and NIR-ASiP[j]

Encouraged by the theoretical calculation and the medium-dependent equilibrium data of ASiP[j], we synthesized several ASiP[j] compounds, by introducing methylamine (ASiP[j] **1**), benzylamine (ASiP[j] **2**) and propargylamine (ASiP[j] **3**) at C-10 of the common julolidine-derived Si-xanthone intermediate (Table 2; for the detailed synthetic procedure, see the ESI†).

Photophysical properties of the new ASiP[j] dyes were measured in different solvents (PBS, ethanol, acetonitrile, and

Table 2 Photophysical properties of ASiP[j] and NIR-ASiP[j] derivatives

ASiP[j]: R₁ = alkyl; R₂ = H
NIR-ASiP[j]: R₁ = alkyl; R₂ = EWG
Julolidine derived dyes

	R_1 (alkyl)	R_2 (EWG)	Solvent	$\lambda_{abs}{}^a$/nm	ε^b/M^{-1} cm^{-1}	$\lambda_{em}{}^c$/nm	$\Phi_F{}^d$
ASiP[j] **1**	Me	H	PBS	481	14 500	655	0.11[e]
			EtOH	487	13 100	628	0.28[e]
			CH$_3$CN	488	12 300	640	0.26[e]
			CH$_2$Cl$_2$	492	18 300	641	0.33[e]
ASiP[j] **2**	Bn	H	PBS	501	13 100	656	0.10[e]
			EtOH	502	14 800	632	0.31[e]
			CH$_3$CN	506	13 900	642	0.30[e]
			CH$_2$Cl$_2$	512	15 900	645	0.32[e]
ASiP[j] **3**	Propargyl	H	PBS	509	26 100	662	0.12[e]
			EtOH	510	20 900	644	0.19[e]
			CH$_3$CN	515	32 000	654	0.18[e]
			CH$_2$Cl$_2$	517	30 200	657	0.23[e]
NIR-ASiP[j] **1**	Me	CO$_2$Bn	PBS	702	109 500	715	0.05[f]
			EtOH	702	114 800	717	0.35[f]
			CH$_3$CN	700	107 400	714	0.26[f]
			CH$_2$Cl$_2$	702	102 600	718	0.40[f]
NIR-ASiP[j] **2**	Me	COCH$_3$	PBS	703	43 200	714	0.06[f]
			EtOH	705	58 600	717	0.29[f]
			CH$_3$CN	700	52 700	713	0.25[f]
			CH$_2$Cl$_2$	706	53 700	718	0.35[f]
NIR-ASiP[j] **3**	Me	COCF$_3$	PBS	711	79 500	724	0.04[f]
			EtOH	713	90 600	728	0.27[f]
			CH$_3$CN	711	95 300	726	0.21[f]
			CH$_2$Cl$_2$	715	87 400	730	0.32[f]

[a] Maximum absorption wavelength. [b] Molar extinction coefficient. [c] Maximum emission wavelength. [d] Fluorescence quantum yields determined in CH$_3$CN using [e] fluorescein ($\Phi = 0.95$ in 0.1 M NaOH) or [f] Nile blue ($\Phi = 0.27$ in ethanol) as reference dyes.

dichloromethane) (Table 2 and Fig. S10–S12, ESI†). In PBS, the absorption and emission maxima (λ_{abs} and λ_{em}) of the ASiP[j] dyes are in the range of 481–509 nm and 655–662 nm, respectively. It is notable that, in comparison with the corresponding ASiP[a] analogues ($\lambda_{abs} \sim 450$ nm; $\lambda_{em} \sim 610$ nm) that emit in the yellow to orange wavelength region, ASiP[j] dyes emit in the far-red region ($\lambda_{em} \sim 650$–660 nm), similar to the SiR dyes ($\lambda_{em} \sim 660$ nm). This bathochromic shift to the far-red emission is crucial to avoid the significant autofluorescence from biomolecules in the yellow emission channel in tissue imaging under two-photon excitation conditions.[8,9] An added value of the ASiP[j] dyes is the large Stokes shift ($\Delta\lambda = \sim 175$ nm), a contrasting feature from conventional SiR dyes ($\Delta\lambda = \sim 18$ nm) (Fig. 1b and c).

Moreover, the ASiP[j] dyes also show bright one-photon emission ($\Phi_F = 0.11$–0.33) and good two-photon absorbing properties (TPACS value, $\delta = 113$–122 GM) under excitation at 800 nm. Furthermore, the ASiP[j] dyes show strong fluorescence at acidic as well as neutral pH (pH 3–7); at basic pH (above pH 8), the fluorescence gradually diminishes due to the equilibrium shift to the non-fluorescent imine form (Fig. S13, ESI†).

Similarly to the case of ASiP[a], finally we synthesized several NIR emitting dyes based on ASiP[j]: benzyl carbamate (NIR-ASiP[j] 1), acetamide (NIR-ASiP[j] 2) and trifluoroacetamide (NIR-ASiP[j] 3) derivatives as the representative dyes (Table 2; for the detailed synthetic procedure, see the ESI†). Photophysical properties of the NIR-ASiP[j] dyes were measured in different solvents (PBS, ethanol, acetonitrile, and dichloromethane).

All the NIR-ASiP[j] dyes show large bathochromic shifts in the absorption and emission bands, emitting in the NIR region above 700 nm (Fig. 1c, Table 2 and Fig. S14–S16, ESI†). For example, NIR-ASiP[j] 1 in PBS shows further bathochromic shifts of ~ 30 nm in the absorption and emission bands ($\lambda_{abs} = 702$ nm; $\lambda_{em} = 715$ nm) compared to the corresponding acyclic analogue NIR-ASiP[a] 1 ($\lambda_{abs} = 669$ nm; $\lambda_{em} = 685$ nm). Thus, NIR-ASiP[j] 1 in PBS shows giant bathochromic shifts of ~ 250 nm in the absorbance band and ~ 105 nm in the emission band from those of the corresponding ASiP[a] 1. Also, all the NIR-ASiP[j] dyes show good quantum yields ($\Phi = 0.05$–0.40) (Table 2) and pH-insensitive NIR emission covering a wide range of pH (pH = 2–10) (Fig. S17, ESI†). The latter property is notable in comparison with the pH-dependent fluorescence emission behavior of the ASiP[a] dyes. An interesting observation is that compared to the ASiP[j] dyes ($\Delta\lambda = 153$–174 nm in PBS), the corresponding NIR-ASiP[j] dyes have much smaller Stokes shifts ($\Delta\lambda = 11$–13 nm in PBS). Similarly, the ASiP[a] dyes have large Stokes shifts ($\Delta\lambda = 154$–160 nm in PBS) but the corresponding NIR-ASiP[a] dyes have much smaller Stokes shifts ($\Delta\lambda = 16$–23 nm in PBS).

In comparison with the well-known NIR emitting cyanine dye (Cy 7: IR780) that undergoes fast photo-oxidation, all the new NIR-ASiP[j] dyes show excellent photostability under continuous irradiation at 633 nm (22 μW cm^{-2}), usual CLSM imaging conditions or at 900 nm (145 mW cm^{-2}), and harsh two-photon imaging conditions, both in PBS at pH 7.4 for 10 min (Fig. S19, ESI†).

Bioimaging capabilities of ASiP[j] and NIR-ASiP[j]

Above all, it was our keen concern whether the new NIR-ASiP[j] dyes would have cellular stability or not. We assessed their cellular imaging behavior along with their parent ASiP[j] dyes under one-photon excitation at 488 nm as well as two-photon excitation at 900 nm. Both the ASiP[j] and NIR-ASiP[j] dyes showed little cell toxicity from standard CCK assays (Fig. S20 and S21†). A549 cells incubated with each of the ASiP[j] dyes 1–3 at 1.0 μM show very bright images using CLSM and TPM (Fig. 4a and c). The bio-stability of the NIR-ASiP[j] dyes 1–3 was evaluated using CLSM, by collecting the emissions from two separate channels: (1) a far-red/NIR window (650–800 nm) under
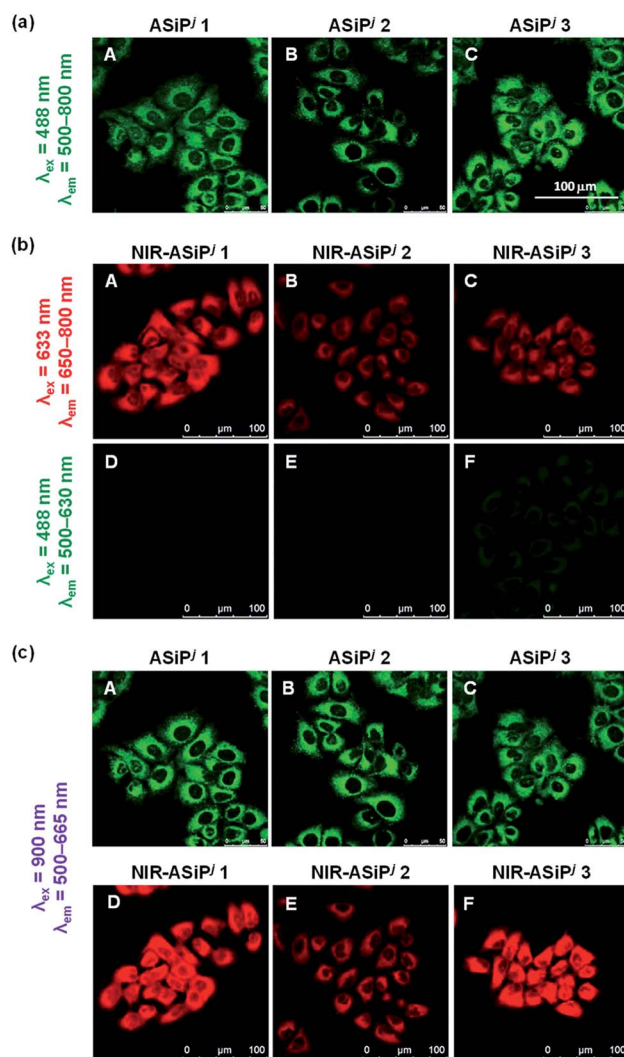

Fig. 4 (a) CLSM images of A549 cells incubated with ASiP[j] dyes (1.0 μM) for 30 min. The images were obtained by excitation at 488 nm and collection of the emissions in the range of 500–800 nm. (b) CLSM images of A549 cells incubated with NIR-ASiP[j] dyes (10 μM) for 30 min. The images were obtained by collecting emissions either from (A–C) the NIR channel (650–800 nm) under excitation at 633 nm or from (D–F) the green channel (500–630 nm) under excitation at 488 nm. (c) TPM images of ASiP[j] (A–C) and NIR-ASiP[j] (D–F) dyes. The images were obtained by excitation at 900 nm and collection of the emissions in the range of 500–665 nm. Scale bar: 100 μm.

excitation at 633 nm, to collect emissions from NIR-ASiP[j] and (2) a shorter wavelength emission window (500–630 nm) under excitation at 488 nm, to collect emissions of any possible decomposed dyes from NIR-ASiP[j]. To our delight, unlike previous NIR-ASiP[a] **1**, the NIR-ASiP[j] dyes **1** and **2** show bright cellular images in the NIR emission window (650–800 nm) (in Fig. 4b, panels A and B) but negligible images in the shorter emission window (in Fig. 4b, panels D and E). Only in the case of the trifluoroacetamide derivative, NIR-ASiP[j] **3**, a slight interference was observed in the short emission window (in Fig. 4b, panel F).

In solution, the julolidine-based NIR-ASiP[j] dyes also showed chemical stability toward Cys and GSH, in contrast to the corresponding NIR-ASiP[a] dyes (Fig. S4†). The results confirm that we have addressed the stability issue by modifying the dye skeleton.

Thus, we can conclude that such NIR-ASiP[j] dyes have biostability sufficient for cellular imaging applications. Furthermore, the new NIR-ASiP[j] dyes provide very bright TPM images under excitation at 900 nm (in Fig. 4c, panels D–F), a commonly accessible wavelength with commercial TPM, which also confirms their strong two-photon absorbing properties.

We also studied the intracellular distribution of the representative NIR-ASiP[j] **1** by co-localization experiments using commercial reference dyes for the nucleus (Hoechst), lysosomes (LysoTracker green) and mitochondria (MitoTracker green), respectively. The results show that NIR-ASiP[j] **1** does not localize in the nucleus (Pearson's correlation coefficient, PCC = −0.30)

and lysosomes (PCC = 0.54) but mostly localizes in the mitochondria (PCC = 0.73), possibly due to the hydrophobic and cationic character (Fig. S22, ESI†).

In short, we have developed Si-pyronin based NIR-emitting dyes (NIR-ASiP[j] dyes) with secured cellular stability. Together with the parent amino-Si-pyronin (ASiP[j]) dyes, the new NIR emitting dyes are photostable, biocompatible, and also provide very bright cellular images under both one- and two-photon excitation conditions. These dyes emit in the far-red or higher wavelength regions, which is crucial for imaging of tissues with minimal autofluorescence interference by TPM.

Launching a unique ratiometric imaging platform through developing a ratiometric probe for H_2O_2

One of our aims in this study was to develop a ratiometric sensing platform based on the ASiP[j]–NIR-ASiP[j] couple. The dye couple would constitute a promising ratiometric sensing system if the latter could be converted into the former triggered by an analyte or other stimuli, which will be accompanied by a considerable spectral shift ($\Delta\lambda > 60$ nm). To demonstrate this scenario, we have prepared a fluorescent probe **ASiP[j]-H_2O_2** (Fig. 5a) having a boronate group, which is well known to react with hydrogen peroxide.[45]

Hydrogen peroxide (H_2O_2), the major reactive oxygen species, is vital to a certain level for normal cell functions such as cell signaling and defense.[46] On the other hand, abnormal generation or accumulation of H_2O_2 can cause several human diseases including cancer and Alzheimer's and Parkinson's
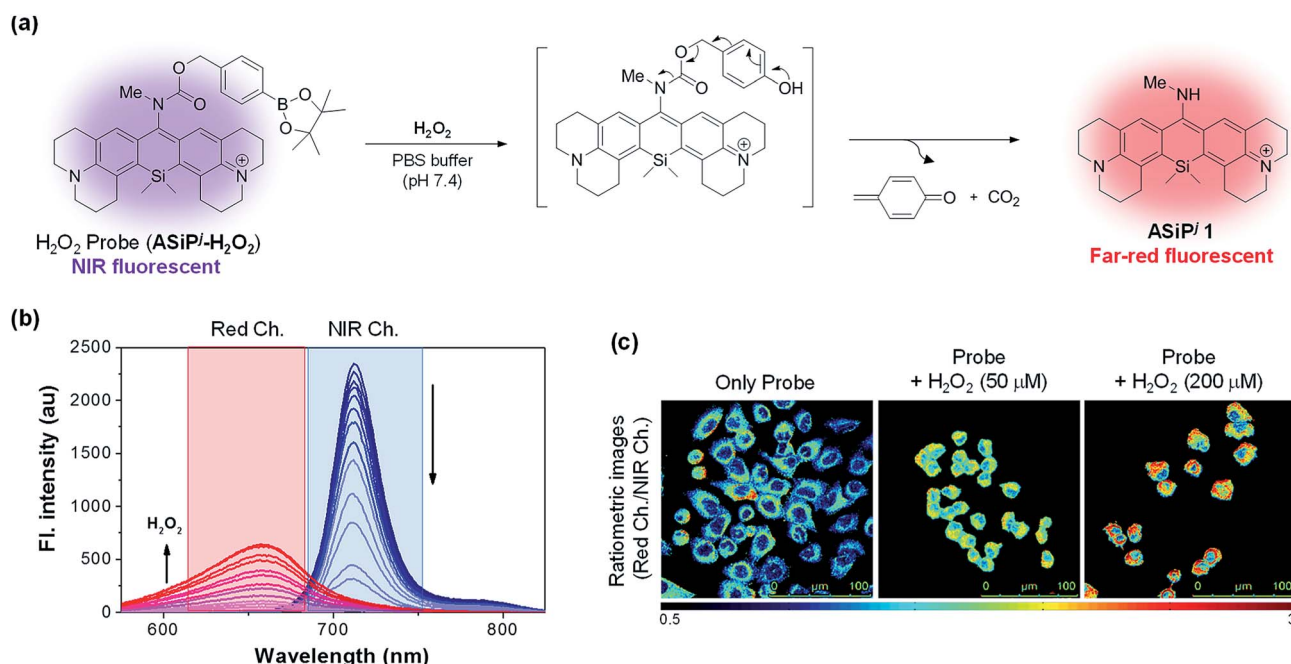

Fig. 5 (a) A ratiometric sensing scheme. (b) Time dependent fluorescence changes of the probe (10 μM) in the presence of H_2O_2 (200 μM) in PBS (10 mM, pH 7.4), showing a gradual decrease of the NIR emission at 712 nm (excitation at 702 nm) with the concomitant increase of the far-red emission at 655 nm (excitation at 481 nm). (c) Ratiometric imaging (I_{Red}/I_{NIR}) of H_2O_2 in A549 cells using the probe: the cells were incubated with either the probe alone (10 μM; incubation for 30 min) or with the probe and exogenously added H_2O_2 (50 and 200 μM; incubation for 30 min). The ratio images (I_{Red}/I_{NIR}) were constructed from the pixel-to-pixel intensity ratio of the images collected in the red channel (500–650 nm, $\lambda_{ex} = 488$ nm) to those collected in the NIR channel (650–800 nm, $\lambda_{ex} = 633$ nm). Scale bar: 100 μm.

diseases.[47,48] Therefore, efficient detection methods of H_2O_2 levels in biological systems are in high demand. In the presence of H_2O_2, the boronate moiety of the NIR emitting probe (**ASiP^j-H_2O_2**) would undergo oxidative cleavage to generate a self-immolative carbamate intermediate, which in turn would undergo spontaneous decarboxylation to generate far-red fluorescent ASiP^j **1** as the product (Fig. 5a). As we expected, the probe emitted in the NIR region with the maximum peak at 712 nm when excited at 702 nm (the wavelength of maximum absorbance) (Fig. 5b). Upon the addition of H_2O_2 to a solution of the probe (10 μM in 10 mM PBS, pH 7.4), the probe peak gradually decreased, while a new emission peak at 655 nm started to increase when excited at 481 nm, the wavelength of maximum absorbance of ASiP^j **1**. The corresponding absorption spectra also showed a gradual shift from the NIR ($\lambda_{abs} = 702$ nm) to visible region ($\lambda_{abs} = 481$ nm) (Fig. S23, ESI†). The fluorescence intensity ratio between the two peaks (I_{655}/I_{712}) showed a linear increase with time as well as with the concentrations of H_2O_2 (Fig. S24–S27, ESI†). The limit of detection was calculated to be as low as 9 nM (Fig. S27†). Thus, the probe is highly sensitive and can be used to detect low concentrations of endogenous H_2O_2 in cells. The probe also showed excellent selectivity towards H_2O_2 over various competing species such as ATP, NAD, metal ions (Fe(III), Fe(II), Zn(II), and Cu(II)), biothiols (GSH and Cys), reactive nitrogen species (NO) and other reactive oxygen species (^{t}BuOOH, ^{t}BuOO$^•$, HO$^•$, and HOCl) (Fig. S28, ESI†). After confirming the excellent sensing properties of the probe in solution, we applied it for the ratiometric imaging of H_2O_2 in A549 cells. The cells were incubated with either the probe alone or with the probe and exogenously added H_2O_2 as a positive control. The images were captured in two separate emission channels: (1) an NIR channel (650–800 nm; $\lambda_{ex} = 633$ nm) for the probe and (2) a red channel (500–650 nm; $\lambda_{ex} = 488$ nm) for the product. The ratio (I_{Red}/I_{NIR}) images were constructed from the pixel-to-pixel intensity ratios of the images collected in the red channel to those collected in the NIR channel. The data show the lowest intensity ratio for the cells treated with the probe alone, but a gradual increase in the intensity ratio as the exogenous H_2O_2 concentration was increased (Fig. 5c).

The results demonstrate that the ASiP^j–NIR-ASiP^j couple provides a novel sensing platform that enables ratiometric cellular imaging of a biological analyte, here H_2O_2, with a minimal spectral overlap through the collection of emissions from NIR to far-red channels, which is promising in that we can minimize the significant autofluorescence from the green and yellow emission channels. By introducing various analyte-specific reactive groups through a self-immolative linker at the 10-amino group of ASiP^j dyes, similarly we could generate ratiometric imaging probes for other analytes of biological importance.

Conclusions

Organic dyes that absorb and emit in the biological optical window (650–950 nm) are in great demand for bioimaging with reduced light scattering and minimal autofluorescence

interference. Only a few classes of such fluorophores are currently available, demanding a new type of far-red/NIR emitting dye. Even rare are those far-red/NIR emitting dyes with two-photon imaging capability. We have developed a novel class of such fluorophores based on a new Si-pyronin dye platform. The introduction of N-acyl or N-alkoxycarbonyl groups on the amine nitrogen of known amino-Si-pyronin dyes causes large bathochromic shifts, leading to the new NIR fluorophores. The promising *in vitro* photophysical properties of the dyes, however, deteriorated in cells, owing to unexpected chemical conversions. This cellular instability issue was eventually solved by changing the known Si-xanthene core into a new julolidine-derived one. The new julolidine-derived amino-Si-pyronin (ASiP^j) and the corresponding NIR-emitting derivatives (NIR-ASiP^j) emit in the far-red and NIR wavelength regions, respectively, afford very bright cellular images, and also have good two-photon absorbing properties. In addition, the new fluorophores are biocompatible, photostable, and have satisfactory water solubility. Furthermore, the NIR-ASiP^j dyes, coupled with the corresponding ASiP^j dyes, offer a unique ratiometric imaging platform that enables bioimaging with minimal spectral overlap, as demonstrated with a ratiometric hydrogen peroxide probe. The new dye systems thus hold great promise for bioimaging application and for the development of ratiometric imaging probes.

Experimental section

The detailed experimental procedures for the measurement of one-photon and two-photon photophysical properties, cell viability assay, and synthesis and characterization data of the new dyes and probe (NMR and HR-mass spectra) are provided in the ESI.† Only the synthetic procedures of NIR-ASiP^j **1–3** are described here.

Synthesis of NIR-ASiP^j 1

A solution of ASiP^j **1** (30 mg, 0.05 mmol) in anhydrous dichloromethane (5 mL) at 0 °C was treated with diisopropylethylamine (44 μL, 0.25 mmol) and pyridine (40 μL, 0.5 mmol), and the mixture was stirred for 10 min at 0 °C followed by the addition of benzyl chloroformate (71 μL, 0.5 mmol). The reaction mixture, after being stirred at room temperature for 3 h, was diluted with dichloromethane and washed with 1 N HCl. The organic layer was evaporated and the residue was subjected to flash column chromatography (eluent: CH_2Cl_2/MeOH = 95/5) to afford the product, which was further purified by preparative HPLC (XBD-C18; gradient 30/70–100/0 A : B over 40 min, A = acetonitrile, B = 0.1% TFA in water, flow rate = 20 mL min^{-1}) to obtain the pure product (4 mg, 11%) as a green solid. ^{1}H NMR (500 MHz, CD$_3$OD, 298 K, δ): 7.25–7.21 (m, 3H), 7.10–7.05 (m, 4H), 5.04 (s, 2H), 3.61–3.57 (m, 8H), 3.22 (s, 3H), 2.96–2.94 (m, 4H), 2.72–2.68 (m, 2H), 2.62–2.58 (m, 2H), 2.06–2.05 (m, 4H), 1.97–1.96 (m, 4H), and 0.67 (d, J = 6.0 Hz, 6H); ^{13}C NMR (125 MHz, CD$_3$OD, 298 K, δ): 161.0, 160.5, 157.2, 157.1, 152.0, 142.9, 142.7, 138.3, 137.9, 135.2, 133.4, 129.9, 129.7, 129.6, 129.5, 129.2, 128.9, 126.6, 125.9, 125.7, 69.2, 68.8, 53.1, 52.5, 40.0, 39.8,

33.2, 30.9, 30.6, 30.1, 28.9, 28.8, 26.2, 22.1, 21.9, 14.6, −0.7, and −0.8; HRMS (ESI) m/z: $[M]^+$ calcd for $C_{36}H_{42}N_3O_2Si^+$, 576.3046; found, 576.3042.

Synthesis of NIR-ASiP[j] 2

A solution of ASiP[j] **1** (30 mg, 0.05 mmol) in anhydrous dichloromethane (5 mL) at 0 °C was treated with 2,6-lutidine (87 µL, 0.75 mmol) and stirred for 10 min at 0 °C, followed by the addition of acetyl chloride (36 µL, 0.5 mmol). The resulting mixture, after being stirred at room temperature for 12 h, was diluted with dichloromethane and washed with 1 N HCl. The organic layer was evaporated and the residue was subjected to column chromatography (eluent: $CH_2Cl_2/MeOH = 95/5$) to afford the product, which was further purified by preparative HPLC (XBD-C18; gradient 30/70–100/0 A : B over 40 min, A = acetonitrile, B = 0.1% TFA in water, flow rate = 20 mL min^{-1}) to obtain the pure product (5 mg, 15%) as a green solid. ^{1}H NMR (500 MHz, CD$_3$OD, 298 K, δ): 7.10 (s, 2H), 3.63–3.60 (m, 8H), 3.22 (s, 3H), 2.98–2.95 (m, 4H), 2.79–2.77 (m, 4H), 2.09–2.06 (m, 4H), 2.03–2.00 (m, 4H), 1.83 (s, 3H), and 0.68 (s, 6H); ^{13}C NMR (125 MHz, CD$_3$OD, 298 K, δ): 173.0, 160.2, 152.2, 142.6, 134.7, 134.0, 127.2, 125.4, 53.2, 53.1, 52.6, 39.1, 30.1, 28.9, 22.0, 21.9, and −0.8; HRMS (ESI) m/z: $[M]^+$ calcd for $C_{30}H_{38}N_3OSi^+$, 484.2784; found, 484.2781.

Synthesis of NIR-ASiP[j] 3

A solution of ASiP[j] **1** (30 mg, 0.05 mmol) in anhydrous dichloromethane (10 mL) at 0 °C was treated with diisopropylethylamine (44 µL, 0.25 mmol) and stirred for 10 min at 0 °C, followed by the addition of trifluoroacetic anhydride (21 µL, 0.15 mmol). The resulting mixture, after being stirred at room temperature for 3 h, was diluted with dichloromethane and washed with 1 N HCl. The organic layer was evaporated and the residue was subjected to column chromatography (eluent: $CH_2Cl_2/MeOH = 95/5$) to afford the product, which was further purified by preparative HPLC (XBD-C18; gradient 30/70–100/0 A : B over 40 min, A = acetonitrile, B = 0.1% TFA in water, flow rate = 20 mL min^{-1}) to obtain the pure product (7 mg, 21%) as a green solid. ^{1}H NMR (500 MHz, CD$_3$OD, 298 K, δ): 7.08 (s, 2H), 3.64–3.62 (m, 8H), 3.40 (s, 3H), 2.98–2.96 (m, 4H), 2.80–2.76 (m, 4H), 2.09–2.06 (m, 4H), 2.01–1.99 (m, 4H), and 0.69 (d, J = 15.0 Hz, 6H); ^{13}C NMR (125 MHz, CD$_3$OD, 298 K, δ): 156.5, 152.2, 142.2, 134.6, 134.2, 134.0, 133.9, 127.1, 127.1, 125.5, 123.6, 57.6, 53.3, 53.2, 52.6, 41.6, 30.9, 30.1, 28.9, 28.8, 22.0, 21.9, −0.7, and −1.0; HRMS (ESI) m/z: $[M]^+$ calcd for $C_{30}H_{35}F_3N_3OSi^+$, 538.2502; found, 538.2505.

Conflicts of interest

The authors are listed as co-inventors of a patent application related to the technology described in this work.

Acknowledgements

Notes and references

1 C. K. Rosenthal, *et al.*, *Nat. Cell Biol.*, 2009, **11**, 1165.
2 J. Zhang, R. E. Campbell, A. Y. Ting and R. Y. Tsien, *Nat. Rev. Mol. Cell Biol.*, 2002, **3**, 906.
3 R. Weissleder, *Nat. Biotechnol.*, 2001, **19**, 316.
4 J. V. Frangioni, *Curr. Opin. Chem. Biol.*, 2003, **7**, 626.
5 L. D. Lavis and R. T. Raines, *ACS Chem. Biol.*, 2014, **9**, 855.
6 J. B. Pawley, *Handbook of confocal microscopy*, Plenum Press, NY, USA, 2nd edn, 1995.
7 A. H. Herz, *Photogr. Sci. Eng.*, 1974, **18**, 323.
8 Y. W. Jun, H. R. Kim, Y. J. Reo, M. Dai and K. H. Ahn, *Chem. Sci.*, 2017, **8**, 7696.
9 D. Kim, H. Moon, S. H. Baik, S. Singha, Y. W. Jun, T. Wang, K. H. Kim, B. S. Park, J. Jung, I. Mook-Jung and K. H. Ahn, *J. Am. Chem. Soc.*, 2015, **137**, 6781.
10 Y. Koide, Y. Urano, K. Hanaoka, T. Terai and T. Nagano, *ACS Chem. Biol.*, 2011, **6**, 600.
11 M. Fu, Y. Xiao, X. Qian, D. Zhao and Y. Xu, *Chem. Commun.*, 2008, 1780.
12 T. Ikeno, T. Nagano and K. Hanaoka, *Chem.–Asian J.*, 2017, **12**, 1435.
13 Y. Koide, Y. Urano, K. Hanaoka, W. Piao, M. Kusakabe, N. Saito, T. Terai, T. Okabe and T. Nagano, *J. Am. Chem. Soc.*, 2012, **134**, 5029.
14 T. Wang, Q.-J. Zhao, H.-G. Hu, S.-C. Yu, X. Liu, L. Liu and Q.-Y. Wu, *Chem. Commun.*, 2012, **48**, 8781.
15 T. Egawa, K. Hanaoka, Y. Koide, S. Ujita, N. Takahashi, Y. Ikegaya, N. Matsuki, T. Terai, T. Ueno, T. Komatsu and T. Nagano, *J. Am. Chem. Soc.*, 2011, **133**, 14157.
16 Y. Kushida, T. Nagano and K. Hanaoka, *Analyst*, 2015, **140**, 685.
17 Y. Gabe, T. Ueno, Y. Urano, H. Kojima and T. Nagano, *Anal. Biochem.*, 2006, **386**, 621.
18 M. Beija, C. A. M. Afonso and J. M. G. Martinho, *Chem. Soc. Rev.*, 2009, **38**, 2410.
19 Z. Mao, H. Jiang, X. Song, W. Hu and Z. Liu, *Anal. Chem.*, 2017, **89**, 9620.
20 D. Kim, H. G. Ryu and K. H. Ahn, *Org. Biomol. Chem.*, 2014, **12**, 4550.
21 H. M. Kim and B. R. Cho, *Chem. Rev.*, 2015, **115**, 5014.
22 J. Bañuelos, V. Martín, C. F. A. Gómez-Durán, I. J. A. Córdoba, E. Peña-Cabrera, I. García-Moreno, Á. Costela, M. E. Pérez-Ojeda, T. Arbeloa and Í. L. Arbeloa, *Chem.–Eur. J.*, 2011, **17**, 7261.
23 H. Zhang, J. Liu, Y.-Q. Sun, Y. Huo, Y. Li, W. Liu, X. Wu, N. Zhu, Y. Shi and W. Guo, *Chem. Commun.*, 2015, **51**, 2721.
24 X. Zhou, Y. Zeng, C. Liyan, X. Wu and J. Yoon, *Angew. Chem., Int. Ed.*, 2016, **55**, 4729.

25 K. N. Bobba, M. Won, I. Shim, N. Velusamy, Z. Yang, J. Qu, J. S. Kim and S. Bhuniya, *Chem. Commun.*, 2017, **53**, 11213.

26 Y. W. Jun, T. Wang, S. Hwang, D. Kim, D. Ma, K. H. Kim, S. Kim, J. Jung and K. H. Ahn, *Angew. Chem., Int. Ed.*, 2018, **57**, 10142.

27 P. Horváth, P. Šebej, T. Šolomek and P. Klán, *J. Org. Chem.*, 2015, **80**, 1299.

28 K. H. Ahn, H. G. Ryu, Y. W. Jun, K. H. Kim and S. Singha, One- or two-photon absorbing fluorescent dyes based on amino-Si-pyronin compound and the uses thereof, KOR 10-2017-0110708, 2017.

29 A. N. Butkevich, G. Lukinavičius, E. D'Este and S. W. Hell, *J. Am. Chem. Soc.*, 2017, **139**, 12378.

30 H. Zhang, J. Liu, L. Wang, M. Sun, X. Yan, J. Wang, J.-P. Guo and W. Guo, *Biomaterials*, 2018, **158**, 10.

31 W. Sun, S. Guo, C. Hu, J. Fan and X. Peng, *Chem. Rev.*, 2016, **116**, 7768.

32 H. Lu, J. Mack, Y. Yang and Z. Shen, *Chem. Soc. Rev.*, 2014, **43**, 4778.

33 H. Chen, B. Dong, Y. Tang and W. Lin, *Acc. Chem. Res.*, 2017, **50**, 1410.

34 T. Ikeno, T. Nagano and K. Hanaoka, *Chem.–Asian J.*, 2017, **12**, 1435.

35 M. H. Lee, J. S. Kim and J. L. Sessler, *Chem. Soc. Rev.*, 2015, **44**, 4185.

36 J. Tang, Z. Guo, Y. Zhang, B. Bai and W.-H. Zhu, *Chem. Commun.*, 2017, **53**, 10520.

37 K. Umezawa, M. Yoshida, M. Kamiya, T. Yamasoba and Y. Urano, *Nat. Chem.*, 2017, **9**, 279.

38 H. Nie, L. Qiao, W. Yang, B. Guo, F. Xin, J. Jing and X. Zhang, *J. Mater. Chem. B*, 2016, **4**, 4826.

39 G. Lukinavičius, K. Umezawa, N. Olivier, A. Honigmann, G. Yang, T. Plass, V. Mueller, L. Reymond, I. R. Corrêa Jr, Z.-G. Luo, C. Schultz, E. A. Lemke, P. Heppenstall, C. Eggeling, S. Manley and K. Johnsson, *Nat. Chem.*, 2013, **5**, 132.

40 A. N. Butkevich, G. Y. Mitronova, S. C. Sidenstein, J. L. Klocke, D. Kamin, D. N. H. Meineke, E. D'Este, P.-T. Kraemer, J. G. Danzl, V. N. Belov and S. W. Hell, *Angew. Chem., Int. Ed.*, 2016, **55**, 3290.

41 G. Lukinavičius, L. Reymond, K. Umezawa, O. Sallin, E. D'Este, F. Göttfert, H. Ta, S. W. Hell, Y. Urano and K. Johnsson, *J. Am. Chem. Soc.*, 2016, **138**, 9365.

42 A. N. Butkevich, V. N. Belov, K. Kolmakov, V. V. Sokolov, H. Shojaei, S. C. Sidenstein, D. Kamin, J. Matthias, R. Vlijm, J. Engelhardt and S. W. Hell, *Chem.–Eur. J.*, 2017, **23**, 12114.

43 S.-N. Uno, M. Kamiya, T. Yoshihara, K. Sugawara, K. Okabe, M. C. Arhan, H. Fujita, T. Funatsu, Y. Okada, S. Tobita and Y. Urano, *Nat. Chem.*, 2014, **6**, 681.

44 E. Kozma, G. E. Girona, G. Paci, E. A. Lemke and P. Kele, *Chem. Commun.*, 2017, **53**, 6696.

45 D. Srikun, E. W. Miller, D. W. Domaille and C. J. Chang, *J. Am. Chem. Soc.*, 2008, **130**, 4596.

46 E. A. Veal, A. M. Day and B. A. Morgan, *Mol. Cell*, 2007, **26**, 1.

47 T. Finkel, M. Serrano and M. A. Blasco, *Nature*, 2007, **448**, 767.

48 K. J. Barnham, C. L. Masters and A. I. Bush, *Nat. Rev. Drug Discovery*, 2004, **3**, 205.